pubs.acs.org/Biomac

Article

Influence of DIBMA Polymer Length on Lipid Nanodisc Formation and Membrane Protein Extraction

Lauren E. Ball,[‖] Liam J. Riley,[‖] Waled Hadasha, Rueben Pfukwa, Corinne J.I. Smith, Timothy R. Dafforn,* and Bert Klumperman*

Cite This: *Biomacromolecules* 2021, 22, 763−772

Read Online

ACCESS | Metrics & More | Article Recommendations | Supporting Information

ABSTRACT: Polymer-based lipid nanoparticles like styrene-maleic acid lipid particles have revolutionized the study of membrane proteins. More recently, alternative polymers such as poly(diisobutylene-*alt*-maleic acid) (DIBMA) have been used in this field. DIBMA is commonly synthesized via conventional radical copolymerization. In order to study the influence of its chain length on lipid nanodisc formation and membrane protein extraction, we synthesized DIBMA with molar masses varying from 1.2−12 kDa via RAFT-mediated polymerization. For molar masses in the range of 3−7 kDa, the rate of lipid nanodisc formation was the highest and similar to those of poly(styrene-*co*-maleic acid) (SMA) and commercially available DIBMA. ZipA solubilization efficiency was significantly higher than for commercially available DIBMA and similar to SMA (circa 75%). Furthermore, RAFT-made DIBMA with a molar mass of 1.2−3.9 kDa showed a much cleaner separation on SDS−PAGE, without the smearing that is typically seen for SMA and commercially available DIBMA.

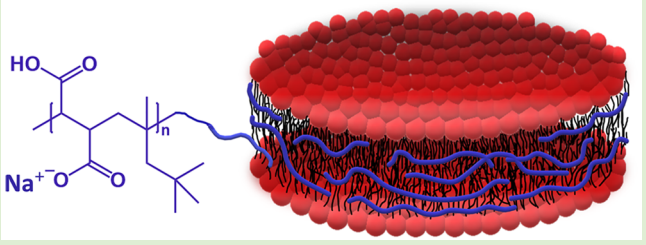

INTRODUCTION

Styrene-maleic acid lipid particles (SMALPs) are stable nanoscale complexes of poly(styrene-*co*-maleic acid) (SMA) and lipids that have a disc-shaped morphology.[1] The complexes assemble in aqueous solution by the intercalation of the phenyl groups of SMA between the acyl chains of lipids perpendicular to the bilayer plane.[2,3] In the last 10 years, these complexes have found significant utility as a support for stabilizing integral membrane proteins.[4−6]

Membrane proteins encapsulated within SMALPs have been shown to be amenable to study by a range of biophysical techniques while maintaining a near-native lipid environment. Insertion into SMALPs has enabled membrane proteins to be studied by a number of methods including circular dichroism spectroscopy, nuclear magnetic resonance spectroscopy, analytical ultracentrifugation,[1] small-angle X-ray and neutron scattering, mass spectroscopy,[7] and cryo-electron microscopy.[5] However, SMA does not represent a universal solution to the study of membrane proteins. The presence of negatively charged maleic acid residues means that the polymer is only soluble at pH > ∼6.4, below this the SMALP dissociates and the polymer precipitates. While this still allows for a study across the physiological pH range, it does preclude use of SMALPs for various techniques, which may require acidic chemistries.[8] SMALP structure is also influenced by divalent cations, which have been shown to bind to the SMALP and cause precipitation of the polymer. Finally, the presence of styrene moieties in the SMA polymer interferes with UV absorbance measurements at 280 nm, a region typically used to determine protein concentrations in solution.[3] These limitations of the SMA copolymer have led to the development of alternative reagents over the past 3 years. The most successful being poly(diisobutylene-*alt*-maleic acid) (DIBMA).[9,10]

DIBMA is a copolymer made up of aliphatic rather than aromatic hydrophobic groups and has been shown to have similar solubilization properties to that of SMA, being capable of extracting proteins directly from cell membranes.[11] The presence of an aliphatic chain instead of the styrene ring seen in SMA confers a number of benefits, a primary one being the lack of interference in spectroscopic studies, allowing for an easier study of membrane proteins solubilized in DIBMA without any contributions toward absorption caused by the polymer belt.

Both the commercial SMA and DIBMA polymers used in membrane protein extraction are produced using conventional radical polymerization, which limits the degree of control over molecular weight distribution (MWD) and chain topology.[12] The broad MWD is because of the probability-based chain growth process with continuous initiation and termination. In contrast, reversible deactivation radical polymerization (RDRP), also known as living radical polymerization, allows

Received: October 26, 2020
Revised: December 11, 2020
Published: December 29, 2020

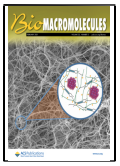

https://dx.doi.org/10.1021/acs.biomac.0c01538
Biomacromolecules 2021, 22, 763−772

Table 1. Conventional Radical Copolymerization Experiments for the Production of DIBMAnh

sample	T (°C)	initiator (mol %)	total conversion (%)	DIB conversion (%)[b]	MAnh conversion (%)[b]	M_n (kDa)[c]	$Đ$
C-D91	70	0.5	24[a]			9.6	2.98
C-D100	80	0.5	46[a]			10.5	2.02
C-D184	80	0.05	75	85	64	19.4	2.10
C-D97	80	1.5	82	92	73	10.2	2.49
C-D62	80	5	97	97	94	6.6	1.96

[a]Conversion determined gravimetrically via precipitation of DIBMAnh in isopropanol. [b]Conversion determined using ^{1}H NMR spectroscopy and an internal reference (1,3,5-trioxane). [c]Molecular weights determined using SEC with DMF as the mobile phase and PMMA calibration standards.

Table 2. RAFT-Mediated Copolymerization Experiments for the Production of DIBMAnh

sample	M_n target (kDa)	total conversion (%)	$M_{n,\,th}$(kDa)[b]	DIB conversion (%)[c]	MAnh conversion (%)[c]	$M_n^{\,SEC}$(kDa)[d]	$M_n^{\,NMR}$(kDa)	$Đ$
R-D12	2.4	39[a]	1.1			1.2	1.3	1.45
R-D20	2.4	63	1.6	71	55	3.2	2.1	1.24
R-D22	2.4	73	1.8	73	72	2.6	2.4	1.28
R-D32	5.4	67	3.8	66	68	2.4	3.4	1.50
R-D37	5.4	64	3.6	64	63	5.5	3.9	1.28
R-D41	5.5	66	3.8	72	61	4.7	4.4	1.33
R-D66	15.0	65	9.9	74	55	9.8	7.0	1.31
R-D88	20.5	22[a]	4.9			9.1	9.3	1.70
R-D96	20.6	33[a]	7.2			13.8	10.1	1.27

[a]Conversion determined gravimetrically via precipitation of DIBMA in isopropanol. [b]Theoretical M_n calculated using individual DIB and MAnh conversions. [c]Conversion determined using ^{1}H NMR spectroscopy and an internal reference (1,3,5-trioxane). [d]Molecular weights determined using SEC with DMF as the mobile phase and PMMA calibration standards.

for the synthesis of well-defined polymeric architectures with narrow MWDs, predetermined molecular weights, and high end-group fidelity as well as allowing for continued chain growth to take place in subsequent polymerization steps. Various types of RDRP are available for the production of well-defined macromolecular architectures, some of which include atom transfer radical polymerization, nitroxide-mediated polymerization, and reversible addition−fragmentation chain transfer polymerization (RAFT). Because of the extensive knowledge that is available regarding the synthesis of SMA via RAFT-mediated polymerization within our research group, RAFT is the RDRP technique of choice for the synthesis of well-defined DIBMA within this article. RAFT allows for precise control over the chain length distribution as the high rate of the addition/fragmentation reactions in comparison with the rate of propagation leads to one or very few monomer additions per activation cycle, resulting in all polymer chains having a similar degree of polymerization.[13] While RAFT polymerization allows for the polymerization of an extensive range of functional monomers, it is important to choose an appropriate chain transfer agent (CTA) by careful selection of the Z- and R-groups of the CTA, in order to achieve successful control over the polymerization. In general, the use of trithiocarbonates and dithiobenzoates works well for the RAFT polymerization of monomers with vinyl groups conjugated to double bonds, such as MAnh and STY. However, a 1,1-dialkyl substituted monomer has not been copolymerized before with maleic anhydride (MAnh) in a RAFT-mediated reaction. The successful RAFT-mediated copolymerization of MAnh with 1-alkenes has previously been reported to yield well-defined polymers through the use of a trithiocarbonate as CTA and thus *S*-butyl-*S*′-(1-phenyl ethyl) trithiocarbonate (BPT) was chosen as the RAFT agent of choice for the polymerization of diisobutylene (DIB) and MAnh.[14] In this article, we exploit the control provided by RAFT polymerization to explore the influence of the DIBMA polymer length on lipid particle formation.

MATERIALS AND METHODS

Materials. Maleic anhydride (MAnh) briquettes (99%, Sigma-Aldrich) and 2,2′-azobis(2-butyronitrile) (AIBN) were purified via recrystallization from toluene and methanol, respectively, and were dried under vacuum overnight. 2,4,4-Trimethyl-1-pentene (diisobutylene, DIB) (99%, Sigma-Aldrich), 2-butanone (≥99%, Sigma-Aldrich), Na_2CO_3 (98%, Merck), 1,3,5-trioxane (≥99%, Sigma-Aldrich), 1-butanethiol (97%, Fluka), carbon disulfide (99%, Sigma-Aldrich), triethylamine (99%, Sigma-Aldrich), 1-bromoethylbenzene (97%. Sigma-Aldrich), $CDCl_3$ (99.9%, MagniSolv), and acetone-d_6 (99.9%, MagniSolv) were used as received. Chloroform was distilled prior to use. The RAFT agent *S*-butyl-*S*′-(1-phenyl ethyl) trithiocarbonate (BPT) was synthesized as described in the literature.[15]

Nomenclature. In all experiments, DIBMA polymers were given a name denoting the method used to synthesize the parent DIBMAnh copolymer (i.e., "R" for RAFT-synthesized and "C-" for conventional free radical copolymerization-synthesized DIBMAnh copolymers) followed by the approximate experimental overall number average degree of polymerization. For example, entry 1, Table 1, that is, C-D91 represents a DIBMAnh parent copolymer prepared by free radical copolymerization with a degree of polymerization, that is, D, of 91, while entry 1 Table 2, that is, R-D12 represents a RAFT-made DIBMAnh parent copolymer with $D \approx 12$.

BPT Synthesis. 1-Butanethiol (5.01 g, 56 mmol), carbon disulphide (8.45 g, 111 mmol), and chloroform (40 mL) were added to a 250 mL round bottom flask fitted with a Teflon coated stirrer bar. Triethylamine (11.22 g, 111 mmol) was added dropwise while stirring and the reaction was allowed to proceed at room temperature for 5 h. 1-Bromoethylbenzene (10.36 g, 56 mmol) was then added dropwise while stirring and the reaction mixture was subsequently allowed to stir overnight under ambient conditions. BPT was isolated from the reaction mixture by successively washing with distilled deionized (DDI) water (2 × 50 mL), H_2SO_4 (2 M, 2 × 50 mL), DDI water (2 × 50 mL), and saturated brine (2 × 50 mL). The mixture was then dried overnight by stirring over anhydrous $MgSO_4$

https://dx.doi.org/10.1021/acs.biomac.0c01538
Biomacromolecules 2021, 22, 763−772

and subsequently filtered and concentrated to yield a viscous yellow−orange oil, (14.84 g, 98%), which was determined to be 96% pure via ^{1}H NMR spectroscopy.

^{1}H NMR (300 MHz, $CDCl_3$): δ = 7.24−7.41 (m, 5H, aromatic), 5.36 (q, J = 5.3 Hz, 1H, −SC**H**−), 3.35 (t, J = 5.7 Hz, 2H, −SC**H**$_2$−), 1.77 (d, J = 5.3 Hz, 3H, −S−CH−C**H**$_3$), 1.68 (q, J = 5.6 Hz, 2H, −CH$_2$−C**H**$_2$−CH$_2$−), 1.43 (sext, J = 5.6 Hz, 2H, −CH$_2$−C**H**$_2$−CH$_3$), 0.94 (t, J = 5.5 Hz, 3H, −CH$_2$−C**H**$_3$).

^{13}C NMR (75 MHz, $CDCl_3$): δ = 14.18 (**C**H$_3$CH$_2$CH$_2$CH$_2$−), 21.93 (**C**H$_3$CH), 22.65 (CH$_3$**C**H$_2$CH$_2$CH$_2$−), 30.58 (CH$_3$CH$_2$**C**H$_2$CH$_2$−), 37.08 (−**C**H$_2$−S), 50.63 (**C**H), 128.22 (*p*-Ph, **C**H), 128.26 (*m*-Ph, **C**H), 129.19 (*o*-Ph, **C**H), 141.73 (Ph, **C**), 223.66 (**C**S$_3$).

General Procedure for the Synthesis of DIBMAnh. In a typical conventional radical copolymerization experiment (Table 1, C-D62), MAnh (3.06 g, 31.2 mmol), DIB (3.50 g, 31.2 mmol), AIBN (0.51 g, 3.1 mmol), 1,3,5-trioxane (0.38 g, 4.2 mmol), and 2-butanone (15 mL) were added to a 50 mL 2-necked pear-shaped flask fitted with a magnetic stirrer bar, condenser, and bubbler. A sample (0.1 mL) was withdrawn at time t = 0. The mixture was degassed by purging with argon gas for 45 min and then submerged in an oil bath at 80 °C for 24 h. At time t = 24 h, a sample (0.1 mL) was withdrawn, and the polymerization was terminated by cooling the flask in an ice-water bath and introducing oxygen into the reaction mixture. For samples C-D91, C-D100, C-D184, and C-D97, the same general procedure was followed but either the temperature was changed (70 °C) or the amount of initiator was changed.

For a typical RAFT polymerization (Table 2, R-D20), MAnh (2.9 g, 30.0 mmol), DIB (3.4 g, 30.1 mmol), AIBN (0.1 g, 0.6 mmol), BPT (0.81 g, 3.0 mmol), 1,3,5-trioxane (0.31 g, 3.5 mmol), and 2-butanone (15 mL) were added to a 3-neck round bottom flask fitted with a magnetic stirrer bar, a condenser, and a bubbler. A sample (0.1 mL) was withdrawn at t = 0 h. The mixture was then degassed by purging with argon gas for 45 min before being immersed in an oil bath at 80 °C for 24 h. At time t = 24 h, a sample (0.1 mL) was withdrawn before the round bottom flask was cooled down in an ice-water bath and the flask was opened to expose the mixture to oxygen. DIBMA was isolated from the reaction mixture by precipitating the copolymer in isopropanol (80 mL) and centrifuging the mixture at 4500 rpm for 5 min in order to obtain the polymer pellet. This pellet was then washed with isopropanol and centrifuged again. The resulting pellet was dried under vacuum at 40 °C and the dry DIBMAnh was analyzed using size exclusion chromatography (SEC), ^{1}H NMR spectroscopy, and attenuated total reflectance infrared spectroscopy (ATR-FTIR) spectroscopy. For samples R-D12, R-D22, R-D32, R-D37, R-D41, R-D66, R-D88, R-D96, R-D37, and R-D54, the same general procedure was followed but either the ratio of BPT to monomer was altered for the production of a variety of molecular weights (calculated using Equation S1, Supporting Information) or the ratio of MAnh and DIB was varied to investigate the alternating nature of the copolymerization. For all RAFT polymerizations, the ratio between the RAFT agent and the initiator of 5:1 was kept constant. A typical kinetic experiment would involve the withdrawal of samples (0.1 mL) under argon at set time intervals (30 min, 1, 2, 4, 6, 8, and 24 h), which were then exposed to air and quenched in liquid nitrogen to terminate polymerization. These samples were then added to deuterated acetone (0.75 mL) and individual monomer conversions were determined using the ^{1}H NMR spectra with 1,3,5-trioxane as the internal standard (eq S2).

General Procedure for the Hydrolysis of DIBMAnh. A stock solution of Na_2CO_3 (1 M, 250 mL) was prepared and used for the hydrolysis of samples C-D62, R-D12, R-D20, R-D32, R-D37, R-D66, R-D88, and R-D96. The DIBMAnh was weighed off into 50 mL round bottom flasks and a calculated volume of the Na_2CO_3 solution was added, such that 2 equiv of Na_2CO_3 to MAnh units were used. These flasks were fitted with magnetic stirrer bars and the mixture was stirred at 80 °C for 24 h. The reaction mixture is initially heterogeneous as DIBMAnh is insoluble in water, thus the complete solubilization of DIBMAnh is an indication of DIBMA production. After 24 h, the contents of the flask were transferred to a dialysis tubing (3500 MWCO) and allowed to stir in water for 1.5 h to remove residual Na_2CO_3. The tube was removed from water and stirred in methanol for 1.5 h resulting in the partial precipitation of DIBMA. This mixture was transferred to a 250 mL round bottom flask and methanol was removed under reduced pressure. The isolated DIBMA was then dried in a vacuum oven at 40 °C for 24 h. The successful production of DIBMA was confirmed via ATR-FTIR spectroscopy and the retention of the RAFT moiety at the chain ends was assessed using UV/vis spectroscopy.

Characterization of DIBMAnh and DIBMA. ^{1}H NMR spectra were obtained using a Varian VXR-Unity (400 MHz) spectrometer. The DIBMAnh copolymers were dissolved in either $CDCl_3$ or acetone-d_6, where the deuterated solvent used is specified with the reported data. ATR-FTIR was performed using a Thermo Scientific Nicolet iS10 Smart iTR with 200 scans over the wavelength range of 600−4000 cm^{-1}. SEC was performed using DMF SEC where all samples made for this analysis are prepared in *N*,*N*-dimethylformamide (DMF) (Sigma-Aldrich, Chromosolv Plus, for HPLC ≥99.9%) with 0.05 M LiBr. The samples were analyzed using a setup consisting of a Waters 717 plus autosampler with a Waters in-line degasser AF connected to a Shimadzu LC-10AT pump. The column setup consisted of a precolumn (1 × PSS GRAM column) with a 10 μm particle size and a dimension of 8.0 × 50 mm; analytical columns 1 × PSS GRAM (10 μm particle size, 100 Å pore size, and 8.0 × 300 mm) and 2 × PSS GRAM columns (10 μm particle size, 3000 Å pore size, and 8.0 × 300 mm). A Waters 410 differential refractometer and a Waters 2487 dual wavelength absorbance detector were connected in series. The flow rate was 0.8 mL/min and the columns were kept at 40 °C. The SEC system was calibrated using low dispersity poly(methyl methacrylate) calibration standards. UV/vis spectra were obtained using a Specord 210 Plus UV/vis spectrophotometer in the wavelength range 190−1100 nm using water as the solvent with a DIBMA concentration of 5 mg/mL.

Solubilization of DMPC Liposomes by DIBMA. A stock solution of 1,2-dimyristoyl-*sn*-glycero-3-phosphocholine [Avanti Polar Lipids; 14:0 PC (DMPC)] liposomes was prepared using a suspension of dry lipid powder in a methanol solution, before evaporation and dissolution to a concentration of 100 mg/mL in 20 mM Tris−HCl, 200 mM NaCl, pH 8.0, this stock solution was stored at −20 °C until use. Liposomes were produced by sonication in a bath sonicator for 1 min, followed by four freeze−thaw cycles and extrusion through a 100 nm filter to generate a sample of homogenous liposomes. Working solutions of DMPC liposomes were produced by dilution of the 100 mg/mL stock solution in 20 mM Tris−HCl, 200 mM NaCl, pH 8.0.

Solutions of SMA and DIBMA were prepared by dissolving the polymers to a concentration of 50 mg/mL in 20 mM Tris−HCl, 200 mM NaCl, and pH 8.0. A 0.5 mg/mL solution of DMPC liposomes was prepared by dilution of the 100 mg/mL DMPC stock solution in 20 mM Tris−HCl, 200 mM NaCl, and pH 8.0, followed by sonication in a bath sonicator for 15 min. Polymer-induced liposome dissolution was monitored by measuring the optical density of 620 nm light of a solution of liposomes using a Cary 100 UV/vis spectrophotometer. A cuvette containing 500 μL of the 0.5 mg/mL liposome solution was placed in the spectrophotometer and allowed to equilibrate for 1 min before the addition of SMA or DIBMA solutions to a final concentration of 0.15 mg/mL. The optical density of the sample was then followed over a period of 10 min. All measurements were performed at 25 °C.

Characterization of DIBMA Nanodiscs. Nanodiscs were produced by addition of SMA or DIBMA in 20 mM Tris−HCl, 200 mM NaCl, pH 8.0 at 5% (w/v) in a 3:1 (w/w) polymer/lipid ratio to DMPC liposomes in 20 mM Tris−HCl, 200 mM NaCl, and pH 8.0 followed by equilibration overnight at 25 °C. Nanodiscs were purified where necessary by means of SEC using an ÄKTA pure protein purification system with a Superdex 200 Increase 10/300 GL (GE Healthcare) equilibrated in 20 mM Tris−HCl, 200 mM NaCl, and pH 8.0 at 4 °C. A flow rate of 0.5 mL/min was used and elution profiles were determined by measuring the absorbance at 280 and 260 nm.

https://dx.doi.org/10.1021/acs.biomac.0c01538
Biomacromolecules 2021, 22, 763−772

Scheme 1. BPT RAFT-Mediated Copolymerization of MAnh and DIB and Subsequent DIBMAnh Hydrolysis Using Aqueous Na_2CO_3 to Produce DIBMA

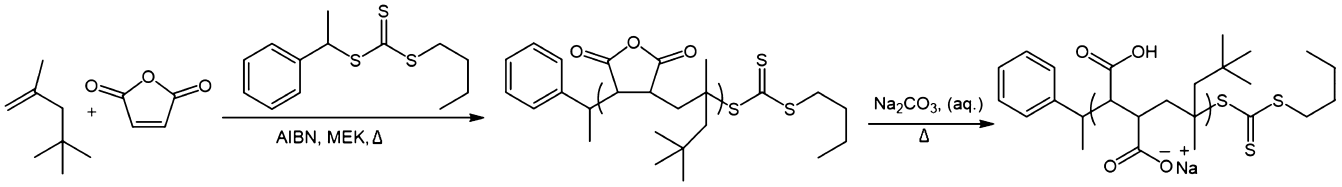

Negatively stained SMA and DIBMA DMPC nanodiscs were visualized with a transmission electron microscope. 5 μL aliquots of nanodiscs produced at 3:1 polymer/lipid were adsorbed to glow-discharged 300 mesh Formvar carbon copper grids (Agar Scientific) and excess sample was removed after 120 s with filter paper (Whatman). Prior to staining, grids were washed with water for 10 s and excess water was removed with filter paper. Grids were stained with 5 μL of 2% (w/v) uranyl acetate for 60 s and excess staining solution was removed with filter paper. Grids were air-dried at room temperature and imaged with a Jeol2100Plus transmission electron microscope operating at an acceleration voltage of 200 kV. Shape factors (diameter and area) of ellipses fitted to particles were analyzed and determined using ImageJ.

Dynamic light scattering (DLS) measurements were conducted using a Malvern Nano S operating with a detector angled at 173° from the incident ray direction. 100 μL aliquots of purified nanodiscs were placed into disposable cuvettes and capped to prevent dust contamination. For each sample, 10 measurements were performed with each being averaged over 10 runs of 10 s. All measurements were performed at 25 °C.

Stability of DIBMA Nanodiscs. *Solubilization of Escherichia coli ZipA Membranes by DIBMA.* *Escherichia coli* membranes were produced as detailed in the article reported by Lee *et al.* (2019)[16] using BL21 Star (DE3) Chemically Competent *E. coli* transformed and induced for high-level expression of His_6-tagged (C-terminus) ZipA in 50 mM Tris−HCl, 500 mM NaCl, 10% glycerol (v/v), and pH 8.0.

Solutions of SMA and DIBMA at 5% (w/v) in resuspension buffer were added to an equal volume of the resuspended pellet and left to incubate at room temperature for 2 h. After incubation 1 mL aliquots of the samples were centrifuged at 100,000×*g* for 45 min to separate soluble and insoluble fractions, insoluble fractions were resuspended in 1 mL resuspension buffer and analyzed by SDS-PAGE and subsequent densitometric analysis was performed in ImageJ.

RESULTS AND DISCUSSION

DIBMAnh Synthesis: Conventional Radical Polymerization. Conventional radical polymerizations were conducted to optimize the reaction conditions for RAFT polymerization in order to maximize monomer conversion. Initially, the reaction temperature was optimized by performing two copolymerizations, one at 70 °C and the other at 80 °C. As expected, the copolymerizations conducted at 80 °C yielded a higher conversion (Table 1) and thus all RAFT polymerizations were performed at this reaction temperature. Variation of the [monomer]/[initiator] ratio for conventional radical polymerizations allowed for the production of DIBMAnh copolymers with different M_n values. The copolymerization that utilized a lower initiator concentration yielded higher M_n values while higher initiator concentrations allowed for the production of lower molecular weight copolymers. ^{1}H NMR spectroscopy was utilized for monomer conversion determination, with the use of an internal reference (1,3,5-trioxane). Upon determination of comonomer conversion for samples C-D184 and C-D97, it was noted that a ∼20% difference in conversion could be observed between MAnh and DIB. This turned out to be because of unintended evaporation of DIB during degassing or during the polymerization. Optimization of the experimental procedure, by ensuring the water running through the condenser was 0 °C, allowed for decreased DIB evaporation, which led to the expected equal conversion of MAnh and DIB (Figure S1, Supporting Information).

DIBMAnh Synthesis: RAFT Polymerization. For RAFT copolymerizations (Scheme 1), different molecular weight samples were synthesized (R-D12, R-D20, R-D22, R-D32, R-D37, R-D41, R-D66, R-D88, and R-D96, Table 2) and copolymerizations were conducted using optimized reaction conditions. For samples R-D12, R-D88, and R-D96, conversion was determined gravimetrically and because of the loss of polymer during this process, reported conversions are significant underestimations of the true values. For all other RAFT experiments, conversion was determined using ^{1}H NMR spectroscopy and relatively high monomer conversions were obtained.

The molecular weight dispersity ($Đ$) of DIBMAnh obtained via RAFT copolymerization was determined to be relatively low suggesting that a narrow distribution of polymer chain lengths was produced. For sample R-D41 (Table 2), a molecular weight of 5500 g/mol was targeted and the polymerization was conducted over 24 h. Samples were taken at specified time intervals and analyzed using SEC and ^{1}H NMR in order to track comonomer conversion, molecular weight, and $Đ$. M_n increased linearly with conversion supporting the livingness of the polymerization system (Figure 1). Based on these results, it was noted that no further increase in molecular weight was achieved after 8 h because of the depletion of AIBN.

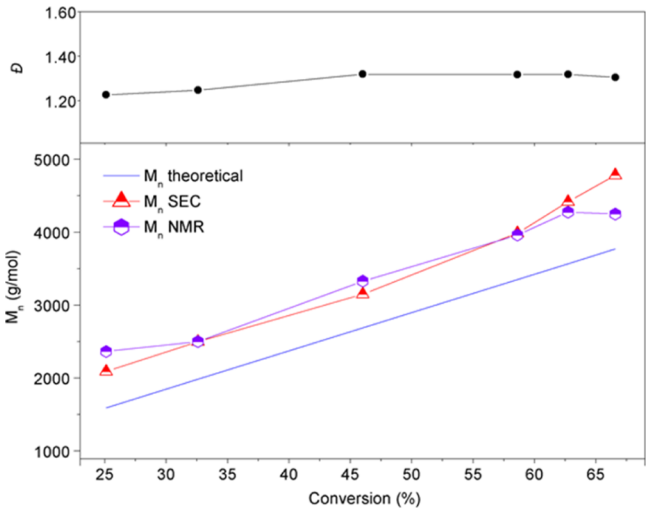

Figure 1. M_n and dispersity vs monomer conversion for the RAFT-mediated polymerization of DIB and MAnh to produce R-D41.

https://dx.doi.org/10.1021/acs.biomac.0c01538
Biomacromolecules 2021, 22, 763−772

A gradual decrease in the SEC elution volume can be observed, with a slight up-turn at high elution volumes as a result of the overlap of the DIBMAnh SEC curve with that of the flow marker (Figure S2). In addition to the gradual increase in molecular weight, the isolated DIBMAnh was shown to have a narrow MWD, thus suggesting that control over the polymerization had been achieved. A difference in comonomer conversion can be observed, because of minimal evaporation of the DIB comonomer, but analysis of the isolated DIBMAnh via ^{1}H NMR spectroscopy revealed an approximately equal number of comonomer units (Figure 2).

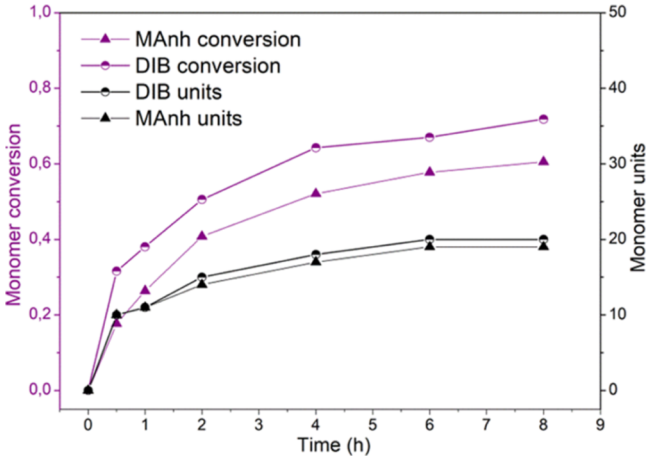

Figure 2. Monomer conversion and monomer units vs time for the RAFT-mediated polymerization of DIB and MAnh to produce R-D41.

A slight discrepancy can be observed when comparing the values obtained for the molecular weight from the ^{1}H NMR and SEC analyses and this can be attributed to the fact that PMMA calibration standards were used, which potentially have a different hydrodynamic volume in solution compared to DIBMAnh. As the molecular weights determined via ^{1}H NMR spectroscopy corresponded well to the theoretical M_n values, these molecular weights were utilized as an indication of polymer chain length in subsequent experiments. Most polymerizations yielded relatively equal comonomer conversions and analysis of the isolated DIBMAnh copolymers using ^{1}H NMR spectroscopy showed approximately equal incorporation of the DIB and MAnh monomers.

This suggests the copolymer is alternating in nature as the comonomers are not expected to homopropagate because of their limited intrinsic reactivity. 1-Alkenes, such as DIB, supposedly are only able to polymerize via RDRP or FRP in the presence of a comonomer with a double bond of significantly different polarity, in this case MAnh, resulting in a polarity activation phenomenon thus allowing for the production of alternating copolymers.[14] To confirm the alternating character of the DIBMAnh copolymers, different comonomer ratios were investigated (Table S1). For both R-D37A and R-D54A, monomer conversion was limited by the altered comonomer ratio and analysis of the isolated DIBMAnh copolymers showed that approximately equal numbers of comonomer units had been incorporated. These results would suggest that all DIBMAnh copolymers are alternating in nature, even when variable comonomer ratios are used. Overall, DIBMAnh copolymers of a variety of molecular weights could be synthesized, producing copolymers of well-defined molecular weight and molecular weight dispersity, both of which play an intrinsic role in the optimization of the membrane solubilization process.

DIBMAnh Hydrolysis. DIBMAnh copolymers C-D62, R-D12, R-D20, R-D32, R-D37, R-D66, R-D88, and R-D96 were converted to DIBMA via the hydrolysis of the MAnh units using Na_2CO_3 (see Scheme 1). The isolated DIBMA copolymers were analyzed using ATR-FTIR spectroscopy. Successful hydrolysis was characterized by the disappearance of the anhydride stretches at 1849 and 1772 cm^{-1}, the appearance of the broad carboxylic acid peak at 3679−3035 cm^{-1}, and the appearance of a carbonyl peak with a shoulder at 1550 and 1660 cm^{-1}, respectively, which arises from the combination of asymmetric and symmetric stretches of carboxylate salts, traditionally found at approximately 1600 and 1400 cm^{-1}, respectively (Figure 3A).

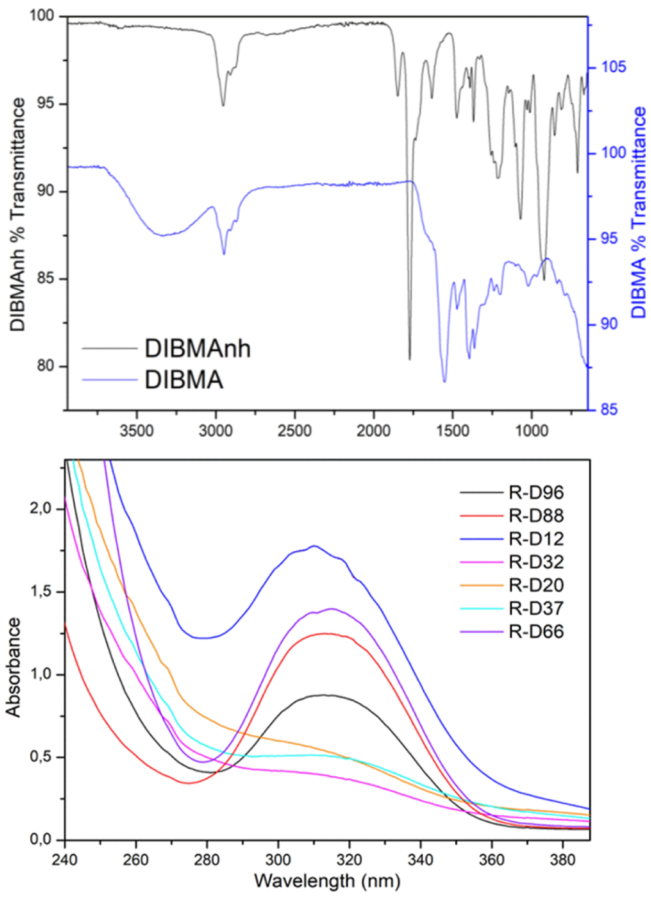

Figure 3. ATR-FTIR comparison between DIBMAnh and DIBMA (top) and UV/vis analysis of DIBMA (bottom).

DIBMA was also analyzed using ^{1}H NMR spectroscopy and the successful hydrolysis of the MAnh units was confirmed via the complete shift of the proton signal from 4.02−3.25 ppm, because of MAnh's methine protons, to 3.17−2.45 ppm, because of maleic acid's methine protons (Figure S3). The hydrolysis of DIBMAnh was carried out under basic aqueous conditions with heating, thus the partial removal of RAFT moieties at the ω-chain ends is not unexpected because of the known hydrolytic instability of RAFT Z end-groups under aqueous alkaline conditions, exacerbated by elevated temperatures.[17] It is likely that the extent to which RAFT moieties are cleaved from DIBMA chains can be influenced by a variety of factors, including the identity of the terminal monomer (i.e.,

https://dx.doi.org/10.1021/acs.biomac.0c01538
Biomacromolecules 2021, 22, 763−772

MAnh or DIB), adjacent to the RAFT Z end-group. As the quantitative analysis of end group retention is not within the scope of this work, a qualitative analysis was conducted via UV/vis spectroscopy. All DIBMA samples analyzed exhibited absorption peaks at ∼310 nm (Figure 3B) because of the $\pi-\pi^*$ transition of the trithiocarbonate moiety of the RAFT Z end-groups,[18] indicating the (partial) retention of the RAFT Z end-groups. The absence of a direct correlation between the DIBMA molar mass and UV peak intensity seems to suggest that the degree of end group retention varies among the different samples.

Analysis of the Performance of DIBMA Variants. To assess the performance of DIBMA variants in the formation of polymer−lipid particles, tests were performed on each sample. These included assessing the rate of solubilization of pure lipid (to produce a nanoparticle). If variants produced lipid nanoparticles, these particles were then analyzed using DLS and electron microscopy to determine if the particle size and shape differed from that formed using the commercial form of DIBMA. The influence of both pH and divalent cation concentration on nanoparticle formation was also assessed. Finally, the efficiency of each polymer in extracting a protein (with a local lipid environment) was measured.

Liposome Dissolution by DIBMA. We initially investigated the membrane-dissolving properties of RAFT DIBMAs to determine the effect, if any, the chain length or the presence of a RAFT group would have on the polymer's ability to solubilize lipids. In order to test this, an assay was developed whereby the decrease in turbidity of a solution of liposomes upon addition of a solubilizing copolymer was measured (Figure 4). The decrease in turbidity is caused by the rapid disruption of the liposomes by the polymer and subsequent formation of smaller nanoscale discs that scatter less light (and hence have a lower turbidity).[19] Alongside comparisons of RAFT DIBMAs, commercial samples of DIBMA and SMA were also analyzed to allow comparisons between our synthesized polymers and those more readily available commercially. Data in Figure 4 show the rapid decrease in scattered light of a solution of 1,2-dimyristoyl-*sn*-glycero-3-phosphocholine (DMPC) liposomes upon addition of copolymers at t = 40 s.

$$\frac{OD_{620}}{OD_{620}^{t=0}} = 1 - C_f e^{-k_f t} - C_s e^{-k_s t} \quad (1)$$

All RAFT DIBMAs show an initial rapid decrease in the turbidity of the solutions, followed by a longer phase of a slower gradual decline; this biphasic behavior was modeled to determine rate constants, with all solubilizations best described by a two-phase decay model in comparison to a one-phase decay model (Figure 4b). The resulting rate constants for each phase (k_f and k_s) were calculated to allow for comparison between polymers. Commercially available SMA (SMA2000P, Cray Valley) and DIBMA (Sokalan-derived) were also analyzed and show the same biphasic decrease in turbidity as the RAFT DIBMAs. k_s values for all RAFT DIBMAs, as well as SMA and Sokalan-derived DIBMA show no significant difference in the solubilization rate, while k_f values vary more considerably among the different polymers. Figure 4c shows the k_f values of RAFT DIBMAs plotted as a function of their M_n. It can be seen that the rate is initially high with a k_f of ∼7.5 min^{-1} for the shortest chain DIBMA R-D12. This value then appears to drop and stabilize in polymers with M_n 2100−7000

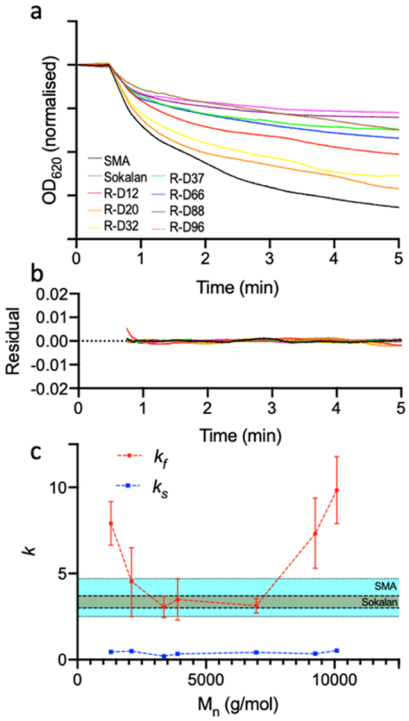

Figure 4. Turbidimetric analysis of solubilization of DMPC liposomes by amphipathic copolymers. (a) Optical density traces for DMPC liposomes upon addition of SMA, Sokalan-derived DIBMA, and RAFT DIBMAs of increasing M_n. Liposomes were allowed to equilibrate before addition of copolymer at t = 40 s. A two-phase decay model was used to fit the data (eq 1) with (b) showing the resulting residuals and (c) representing the rate constants derived from the fitted data plotted as a function of the M_n of the RAFT DIBMA used in solubilization. Points represent the mean of three experiments with error bars representing the standard error of the mean (SEM). The SEM of k_f of SMA and Sokalan are represented as the cyan- and brown-highlighted regions, respectively.

g/mol to a k_f of ∼4 min^{-1}. Long-chain RAFT DIBMAs R-D88 and R-D96 show increased k_f values also, similar to the shortest chain DIBMA R-D12. Interestingly, rates for R-D20, R-D32, R-D37, and R-D66 are comparable with those of SMA2000P and Sokalan-derived DIBMA.

The data in Figure 4 highlight the effect of the polymer chain length on solubilization. It is clear that all RAFT DIBMAs were capable of solubilizing lipids rapidly in a similar manner to SMA. Previous studies in the literature have revealed that SMA solubilization follows an initial rapid step of polymer adsorption to the lipid membrane, followed by membrane disruption.[20] These two phases of solubilization would perhaps, therefore, be represented in this system in the biphasic loss of optical density in vesicles being solubilized by the amphipathic polymers. The initial rapid decrease in turbidity seen in Figure 4a may be indicative of the process of liposome destabilization, thereby causing an initial large drop in turbidity because of a reduction in the amount of light scattered by the now destabilized membranes.

Following destabilization, SMA nanodiscs are formed and stabilized by the burial of the phenyl groups into the acyl core of the phospholipid bilayer; while DIBMA is stabilized in a similar manner using its hydrophobic alkyl chains.[2] The second phase of the model may represent this gradual approach to a homogenous set of discs with a narrow size distribution, driven by lipid exchange among discs.[21] The sharing of the biphasic

https://dx.doi.org/10.1021/acs.biomac.0c01538
Biomacromolecules 2021, 22, 763−772

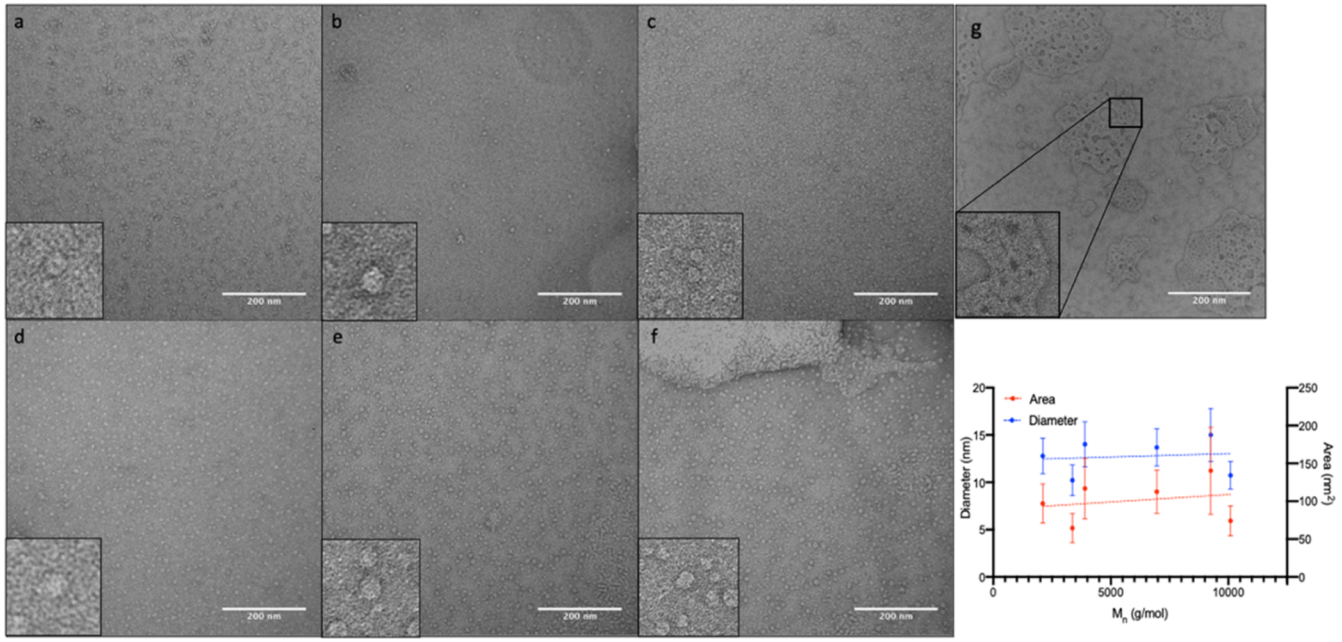

Figure 5. Representative transmission electron micrograph (TEM) of DMPC liposomes solubilized using RAFT DIBMAs (a) R-D20, (b) R-D32, (c) R-D37, (d) R-D66, (e) R-D88, (f) R-D96, and (g) R-D12. Magnified images show representative single particles of RAFT DIBMA DMPC nanodiscs from the micrograph. DMPC−DIBMALPs were prepared by addition of polymer to DMPC liposomes at a 3:1 polymer to lipid ratio and incubated for 24 h to allow for complete solubilization and nanodisc formation. Samples were then negatively stained using uranyl acetate and imaged at 60k×. (h) Size distribution analysis of DMPC−DIBMALP sizes imaged with the transmission electron microscope plotted as a function of RAFT DIBMA M_n. Points represent the mean frequency of sizes of 250 particles with error bars showing ±1 standard deviation.

solubilization profile seen in Figure 4a by both SMA and DIBMA provides further evidence that the driving forces behind the mechanism of solubilization by these polymers are also shared.

DIBMA Nanoparticle Characterization. DLS experiments were also performed as an orthogonal technique to TEM for determining the size of nanoparticles. Data in Figure 6a show the intensity-based distribution of nanoparticles formed using DMPC and RAFT DIBMAs, the data show a narrow size distribution of particles with *Z*-averages ranging from 11−23 nm, in agreement with TEM-derived particle sizes and with previous reports using DIBMA.[10] DLS measurements of R-D12 revealed a heterogeneous range of particles from 7−210 nm. The results here support the idea that the sample consists of a mixture of nanodiscs and disrupted vesicles, as visualized using the transmission electron microscope and seen in Figure 5g; this corroborates with findings in a similar system using fractionated DIBMA from a commercial source wherein all but the shortest polymer chains were capable of solubilizing and forming nanodiscs.[10]

The presence of pores in vesicles in samples made using R-D12 show that while the polymer is capable of entering and solubilizing membranes (Figure 5), it is incapable of producing a homogenous sample of nanodiscs as seen with other similar polymers (Figure 5g), the reduction in chain length appears to result in the inability for nanodiscs to separate from the larger pore-containing membrane structures. Therefore, we believe that these pore-containing vesicles represent an intermediary step in liposome solubilization by amphipathic copolymers, with studies in the literature also showing the capability of SMA to form pores in biomembranes[22] as a potential precursor for nanodisc formation. Similar studies have also suggested that the formation of lipid discs can follow an island-formation pathway,[23] whereby small pores induced by the copolymer

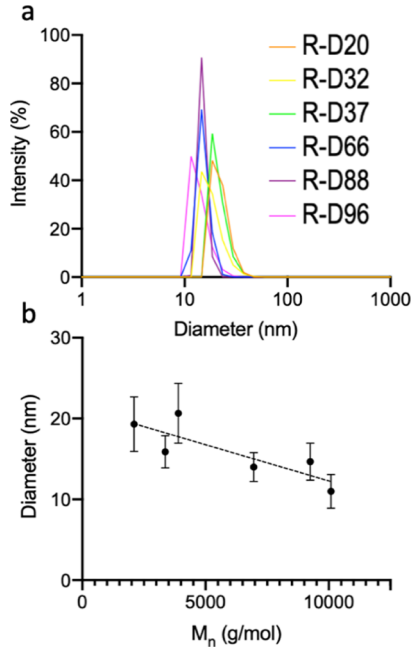

Figure 6. Structural analysis of DMPC−DIBMALP nanodiscs using DLS. (a) Intensity-based distributions of DMPC liposomes solubilized using RAFT DIBMAs of varying M_n. DMPC−DIBMALPs were prepared by addition of polymer to DMPC liposomes at a 3:1 polymer to lipid ratio and incubated for 24 h to allow for complete solubilization and nanodisc formation before DLS measurement. DLS measurements are the result of 10, 1 s accumulations. (b) Hydrodynamic diameter of DMPC−DIBMALPs plotted as a function of the copolymer M_n, points represent the mean of three experiments with error bars representing ±1 standard deviation.

https://dx.doi.org/10.1021/acs.biomac.0c01538
Biomacromolecules 2021, 22, 763−772

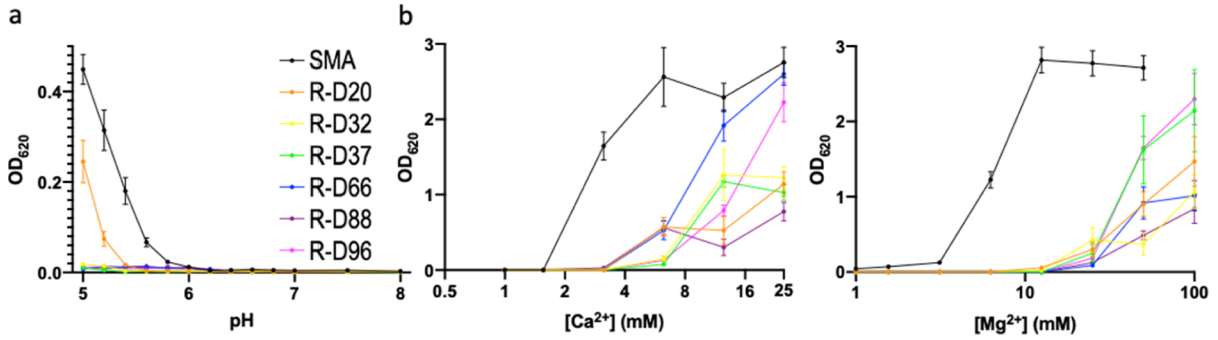

Figure 7. Analysis of RAFT DIBMALP stability. (a) Turbidity of DIBMALP solutions as a function of pH, nanodiscs were prepared by addition of the polymer to DMPC liposomes at a 3:1 polymer to lipid ratio in 50 mM Tris and 150 mM NaCl and incubated for 24 h to allow for complete solubilization and nanodisc formation. (b) Turbidity of DIBMALP solutions as a function of calcium and magnesium ion concentration. Points represent the mean value taken from three separate experiments with error bars displaying SEM.

eventually merge to leave a lipid disc, which is capable of moving out of the bilayer as a lipid−copolymer complex.

One of the primary limitations of SMA is its low tolerance for divalent cations, as well as insolubility at low pH, these limitations can prevent proteins encapsulated in SMALPs from being investigated using various downstream biochemical methods. In order to assess the stability of our RAFT DIBMA nanodiscs, an assay was developed wherein solutions of nanodiscs were exposed to varying environmental conditions (pH, $[Ca^{2+}]$, and $[Mg^{2+}]$) and the turbidity of the solution was measured. Nanodisc solutions that show an increased turbidimetric signal indicate nanodisc destabilization because of precipitation of the polymer and subsequent precipitation of lipid components from the nanodisc phase. Data in Figure 7a show that nanodiscs formed using R-D20, the second lowest M_n RAFT DIBMA, show stability to pH 5.5, with all other RAFT DIBMAs remaining stable to pH 5. In this experiment, SMA acted as a control and precipitated at approximately pH 6, which is consistent with data for SMA-based nanodiscs in the literature.[24] The data from Figure 7b and c show the sensitivity of RAFT DIBMA nanodiscs to solutions containing the divalent cations magnesium and calcium. All RAFT DIBMA copolymer nanodiscs were resistant to magnesium ions up to a concentration of 8 mM, with SMA-based nanodiscs sensitive to low concentrations of magnesium (<1 mM). In the case of calcium, all RAFT DIBMAs, however, showed increased resistance compared to SMA by remaining stable with up to 4 mM calcium ions in solution.

DIBMA Solubilization of Membrane Proteins from *E. coli*. Both SMA and DIBMA have been shown to be capable of solubilizing membrane proteins directly from biological membranes. We, therefore, investigated the efficiency of our RAFT DIBMAs to solubilize *E. coli* membranes overexpressed for cell division protein ZipA; having been extensively characterized in SMA previously.[16] The solubilizing ability of RAFT DIBMAs was compared to commercially available SMA2000P and Sokalan, both already commonly utilized in solubilizing functional membrane proteins.

After solubilization of the membranes by the various polymers for 24 h, soluble and insoluble fractions were separated by ultracentrifugation and analyzed by SDS-PAGE (Figure 8a). Samples that successfully solubilized ZipA will produce a band that migrates with an apparent mass of approximately 50 kDa. It should be noted that despite ZipA having a mass of <40 kDa, ZipA is known to migrate aberrantly

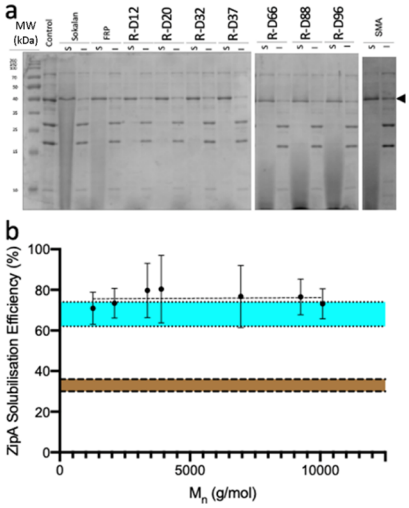

Figure 8. Solubilization of membrane proteins using RAFT DIBMA copolymers. (a) Coomassie-stained SDS-PAGE showing proteins both solubilized (S) and remaining insoluble (I) after incubation of *E. coli* membranes (transformed for overexpression of the trans-membrane protein ZipA) with Sokalan-derived DIBMA, conventional radical polymerization (FRP) of DIBMA and RAFT DIBMAs of increasing M_n. The black arrow is representative of the ZipA band and a control using total insoluble protein prior to addition of copolymer is also shown. (b) Densitometric analysis of SDS-PAGE showing efficiency of solubilization of the protein ZipA. Solubilization efficiency is expressed as a percentage of total insoluble ZipA, with error bars representing the SEM of three separate experiments.

through SDS-PAGE gels giving an apparent mass of 40 kDa.[16,25,26]

RAFT DIBMA-solubilized samples were all shown capable of solubilizing ZipA, with all lanes containing soluble material presenting a band of ∼40 kDa. Densitometric analysis of the SDS-PAGE gel (Figure 8b) reveals a solubilization efficiency for the *E. coli* protein ZipA of ∼75% for all RAFT DIBMAs, with no statistically significant difference in solubilization efficiency found among the polymer samples. Solubilization efficiency was also similar among RAFT DIBMAs and SMA2000P. The commercially available form of DIBMA, however, is the least efficient at solubilizing ZipA, with an efficiency of ∼30%. This lower efficiency for Sokalan-derived DIBMA has previously been reported in studies comparing SMA and DIBMA and is further corroborated by the data in Figure 8b showing a reduced rate of solubilization in Sokalan-

https://dx.doi.org/10.1021/acs.biomac.0c01538
Biomacromolecules 2021, 22, 763−772

derived DIBMA compared to SMA. Interestingly, R-D12, R-D20, R-D32, and R-D37 all produce signals from SDS-PAGE free of the smearing characteristics of SDS-PAGE with SMA2000P and Sokalan-derived DIBMA.

Smearing can be seen, however, in the soluble lanes of R-D66, R-D88, and R-D96, with R-D88 also having a $Đ$ of 1.7. The smearing, therefore, is likely caused by incomplete migration of excess polymer present in the sample from the gel. Both commercial SMA and Sokalan-derived DIBMA are copolymers synthesized using conventional radical polymerization, which results in them having a broad MWD, therefore SDS-PAGE gels using these copolymers will likely always maintain smearing because of the presence of high-molecular-weight copolymer chains remaining postsolubilization. The DIBMA copolymers in this study synthesized using RAFT, however, have comparatively narrower MWDs, therefore samples R-D12, R-D20, R-D32, and R-D37 represent samples with a low enough M_n and $Đ$ that the bulk of excess polymer chains is capable of completely migrating through the gel during the electrophoretic process.

CONCLUSIONS

The success of nanoencapsulation systems (like SMALPs or MSPs) for producing membrane proteins in their native environment has been underlined by their use in a steadily increasing number of membrane protein studies. As with any new area that is reliant on a specific reagent, successful application has also led to work on improving the reagent itself. For SMALPs, this has led to a rapid introduction of a number of new polymer derivatives.[23] One of the most successful has been the DIBMA polymer, which has clear advantages over SMA in terms of divalent cation sensitivity. However, only one preparation of DIBMA is currently available and little is known about whether this form represents the optimal solution.

In this contribution, we carried out a systematic analysis of the influence of DIBMA polymer length on nanodisc formation with a view of discovering whether polymer size can influence performance. Our results show that except for the lowest molecular weight, the polymers all form recognizable nanodiscs that in general behave in a similar manner to the commercially available material. Kinetically, we do observe an influence of polymer size with optimum performance being close to a M_n of 5000.

Our studies of protein solubilization again show very similar protein extraction efficiencies for all polymers tested. However, analysis of the PAGE data shows that the lower-molecular-weight polymers interfere less with the staining of the gels. This is an important observation as visualization of the proteins using PAGE is a fundamental part of any protein purification process.

Finally, our EM studies of the morphology of nanodiscs formed using the polymer highlight a somewhat unexpected result that might provide insights into disc formation. The images for the lowest molecular weight polymer show a state of incomplete membrane protein solubilization. Instead of discs, we observe membranes with a "lacey" appearance. Unusually for membranes, we observe holes through the bilayer and on the edges of bilayer fragments, there is evidence of convex regions. It is possible that what we are observing are the initial stages of disc formation where polymer penetrated the bilayer forming holes.[27] In the case of the edges of bilayer fragments, these holes have merged, leading to the production of a fragment. Thus, the edges of the fragment appear to be stabilized by the presence of the polymer.

Overall, our data show that there is a "sweet spot" for DIBMA polymers that facilitate rapid and robust nanodisc formation without perturbing PAGE visualization. We also show initial evidence for the mechanism of DIBMA-mediated nanodisc formation.

ASSOCIATED CONTENT

Supporting Information

The Supporting Information is available free of charge at https://pubs.acs.org/doi/10.1021/acs.biomac.0c01538.

Calculation of monomer conversion from the 1H NMR spectra; conversion and molecular weight data for RAFT copolymerizations performed using varying monomer ratios; individual monomer conversion versus time; SEC curves at different reaction times; and ^{1}H NMR spectra of polymers before and after hydrolysis of MAnh (PDF)

AUTHOR INFORMATION

Corresponding Authors

Timothy R. Dafforn − *School of Biosciences, University of Birmingham, Birmingham B15 2TT, United Kingdom*; Email: t.r.dafforn@bham.ac.uk

Bert Klumperman − *Department of Chemistry and Polymer Science, Stellenbosch University, Stellenbosch 7602, South Africa*; orcid.org/0000-0003-1561-274X; Email: bklump@sun.ac.za

Authors

Lauren E. Ball − *Department of Chemistry and Polymer Science, Stellenbosch University, Stellenbosch 7602, South Africa*

Liam J. Riley − *School of Life Sciences, The University of Warwick, Coventry CV4 7AL, United Kingdom; School of Biosciences, University of Birmingham, Birmingham B15 2TT, United Kingdom*

Waled Hadasha − *Department of Chemistry and Polymer Science, Stellenbosch University, Stellenbosch 7602, South Africa*

Rueben Pfukwa − *Department of Chemistry and Polymer Science, Stellenbosch University, Stellenbosch 7602, South Africa*

Corinne J.I. Smith − *School of Life Sciences, The University of Warwick, Coventry CV4 7AL, United Kingdom*

Complete contact information is available at: https://pubs.acs.org/10.1021/acs.biomac.0c01538

Author Contributions

‖L.E.B. and L.J.R. co-authors contributed equally to this work.

Notes

The authors declare no competing financial interest.

ACKNOWLEDGMENTS

B.K., L.E.B., W.H., and R.P. acknowledge support by the South African Research Chairs Initiative of the Department of Science and Technology (DST) and National Research Foundation (NRF) of South Africa (Grant no. 46855). We acknowledge the Midlands Regional Cryo-EM Facility, hosted at the Warwick Advanced Bioimaging Research Technology Platform, for use of the JEOL 2100Plus, supported by MRC award reference MC_PC_17136.

REFERENCES

(1) Knowles, T. J.; Finka, R.; Smith, C.; Lin, Y.-P.; Dafforn, T.; Overduin, M. Membrane proteins solubilized intact in lipid containing nanoparticles bounded by styrene maleic acid copolymer. *J. Am. Chem. Soc.* **2009**, *131*, 7484−7485.

(2) Jamshad, M.; Grimard, V.; Idini, I.; Knowles, T. J.; Dowle, M. R.; Schofield, N.; Sridhar, P.; Lin, Y.; Finka, R.; Wheatley, M.; Thomas, O. R. T.; Palmer, R. E.; Overduin, M.; Govaerts, C.; Ruysschaert, J.-M.; Edler, K. J.; Dafforn, T. R. Structural analysis of a nanoparticle containing a lipid bilayer used for detergent-free extraction of membrane proteins. *Nano Res.* **2015**, *8*, 774−789.

(3) Tonge, S. R.; Tighe, B. J. Responsive hydrophobically associating polymers: a review of structure and properties. *Adv. Drug Deliv. Rev.* **2001**, *53*, 109−122.

(4) Postis, V.; Rawson, S.; Mitchell, J. K.; Lee, S. C.; Parslow, R. A.; Dafforn, T. R.; Baldwin, S. A.; Muench, S. P. The use of SMALPs as a novel membrane protein scaffold for structure study by negative stain electron microscopy. *Biochim. Biophys. Acta* **2015**, *1848*, 496−501.

(5) Parmar, M.; Rawson, S.; Scarff, C. A.; Goldman, A.; Dafforn, T. R.; Muench, S. P.; Postis, V. L. G. Using a SMALP platform to determine a sub-nm single particle cryo-EM membrane protein structure. *Biochim. Biophys. Acta* **2018**, *1860*, 378−383.

(6) Dörr, J. M.; Koorengevel, M. C.; Schäfer, M.; Prokofyev, A. V.; Scheidelaar, S.; van der Cruijsen, E. A. W.; Dafforn, T. R.; Baldus, M.; Killian, J. A. Detergent-free isolation, characterization, and functional reconstitution of a tetrameric K^+ channel: The power of native nanodiscs. *Proc. Natl. Acad. Sci. U.S.A.* **2014**, *111*, 18607−18612.

(7) Broecker, J.; Eger, B. T.; Ernst, O. P. Crystallogenesis of Membrane Proteins Mediated by Polymer-Bounded Lipid Nanodiscs. *Structure* **2017**, *25*, 384−392.

(8) Cunningham, B. C.; Wells, J. A. Comparison of a structural and a functional epitope. *J. Mol. Biol.* **1993**, *234*, 554−563.

(9) Grethen, A.; Oluwole, A. O.; Danielczak, B.; Vargas, C.; Keller, S. Thermodynamics of nanodisc formation mediated by styrene/maleic acid (2:1) copolymer. *Sci. Rep.* **2017**, *7*, 11517.

(10) Oluwole, A. O.; Klingler, J.; Danielczak, B.; Babalola, J. O.; Vargas, C.; Pabst, G.; Keller, S. Formation of Lipid-Bilayer Nanodiscs by Diisobutylene/Maleic Acid (DIBMA) Copolymer. *Langmuir* **2017**, *33*, 14378−14388.

(11) Oluwole, A. O.; Danielczak, B.; Meister, A.; Babalola, J. O.; Vargas, C.; Keller, S. Solubilization of Membrane Proteins into Functional Lipid-Bilayer Nanodiscs Using a Diisobutylene/Maleic Acid Copolymer. *Angew. Chem., Int. Ed.* **2017**, *56*, 1919−1924.

(12) Moad, G.; Rizzardo, E.; Thang, S. H. Toward living radical polymerization. *Acc. Chem. Res.* **2008**, *41*, 1133−1142.

(13) Perrier, S. 50th Anniversary Perspective: RAFT Polymerization—A User Guide. *Macromolecules* **2017**, *50*, 7433−7447.

(14) Ma, J.; Cheng, C.; Sun, G.; Wooley, K. L. A polarity-activation strategy for the high incorporation of 1-alkenes into functional copolymers via RAFT copolymerization. *J. Polym. Sci., Part A: Polym. Chem.* **2008**, *46*, 3488−3498.

(15) Postma, A.; Davis, T. P.; Evans, R. A.; Li, G.; Moad, G.; O'Shea, M. S. Synthesis of well-defined polystyrene with primary amine end groups through the use of phthalimido-functional RAFT agents. *Macromolecules* **2006**, *39*, 5293−5306.

(16) Lee, S. C.; Collins, R.; Lin, Y.-p.; Jamshad, M.; Broughton, C.; Harris, S. A.; Hanson, B. S.; Tognoloni, C.; Parslow, R. A.; Terry, A. E.; Rodger, A.; Smith, C. J.; Edler, K. J.; Ford, R.; Roper, D. I.; Dafforn, T. R. Nano-encapsulated Escherichia coli Divisome Anchor ZipA, and in Complex with FtsZ. *Sci. Rep.* **2019**, *9*, 18712.

(17) Baussard, J.-F.; Habib-Jiwan, J.-L.; Laschewsky, A.; Mertoglu, M.; Storsberg, J. New chain transfer agents for reversible addition-fragmentation chain transfer (RAFT) polymerisation in aqueous solution. *Polymer* **2004**, *45*, 3615−3626.

(18) Skrabania, K.; Miasnikova, A.; Bivigou-Koumba, A. M.; Zehm, D.; Laschewsky, A. Examining the UV-vis absorption of RAFT chain transfer agents and their use for polymer analysis. *Polym. Chem.* **2011**, *2*, 2074−2083.

(19) Dörr, J. M.; Scheidelaar, S.; Koorengevel, M. C.; Dominguez, J. J.; Schäfer, M.; van Walree, C. A.; Killian, J. A. The styrene-maleic acid copolymer: a versatile tool in membrane research. *Eur. Biophys. J.* **2016**, *45*, 3−21.

(20) Scheidelaar, S.; Koorengevel, M. C.; Pardo, J. D.; Meeldijk, J. D.; Breukink, E.; Killian, J. A. Molecular model for the solubilization of membranes into nanodisks by styrene maleic Acid copolymers. *Biophys. J.* **2015**, *108*, 279−290.

(21) Cuevas Arenas, R.; Danielczak, B.; Martel, A.; Porcar, L.; Breyton, C.; Ebel, C.; Keller, S. Fast Collisional Lipid Transfer Among Polymer-Bounded Nanodiscs. *Sci. Rep.* **2017**, *7*, 45875.

(22) Orwick Rydmark, M.; Christensen, M. K.; Köksal, E. S.; Kantarci, I.; Kustanovich, K.; Yantchev, V.; Jesorka, A.; Gözen, I. Styrene maleic acid copolymer induces pores in biomembranes. *Soft Matter* **2019**, *15*, 7934−7944.

(23) Stroud, Z.; Hall, S. C. L.; Dafforn, T. R. Purification of membrane proteins free from conventional detergents: SMA, new polymers, new opportunities and new insights. *Methods* **2018**, *147*, 106−117.

(24) Hall, S. C. L.; Tognoloni, C.; Price, G. J.; Klumperman, B.; Edler, K. J.; Dafforn, T. R.; Arnold, T. Influence of Poly(styrene- co-maleic acid) Copolymer Structure on the Properties and Self-Assembly of SMALP Nanodiscs. *Biomacromolecules* **2018**, *19*, 761−772.

(25) Mosyak, L.; Zhang, Y.; Glasfeld, E.; Haney, S.; Stahl, M.; Seehra, J.; Somers, W. S. The bacterial cell-division protein ZipA and its interaction with an FtsZ fragment revealed by X-ray crystallography. *EMBO J.* **2000**, *19*, 3179−3191.

(26) Kuchibhatla, A.; Bhattacharya, A.; Panda, D. ZipA binds to FtsZ with high affinity and enhances the stability of FtsZ protofilaments. *PLoS One* **2011**, *6*, No. e28262.

(27) Xue, M.; Cheng, L.; Faustino, I.; Guo, W.; Marrink, S. J. Molecular Mechanism of Lipid Nanodisk Formation by Styrene-Maleic Acid Copolymers. *Biophys. J.* **2018**, *115*, 494−502.

https://dx.doi.org/10.1021/acs.biomac.0c01538
Biomacromolecules 2021, 22, 763−772